ORIGINAL PAPER

Preparation and characterization of graphene nanosheets dispersed pyrrole-chorobenzaldehyde-heptaldehyde conjugated terpolymer nanocomposites for DNA detection

Annamalai Pangajam[1] · Ayyavu Chandramohan[2] · Kannaiyan Dinakaran[1] · Gurusamy Harichandran[3] · R Sureshkumar[4]

Abstract

A new conductive terpolymer/graphene nanosheet hybrid composite has been synthesized by polymerizing pyrrole, chlorobenzaldehyde, and heptaldehyde (PPyCB&H), in the presence of graphene nanosheets (GNS), using *p*-toluene sulfonic acid as a catalyst. Fourier transform infrared spectra, proton nuclear magnetic resonance, transmission electron microscopy, and X-ray diffraction patterns confirm the formation of PPyCB&H/GNS hybrid nanocomposites. Further, the resultant nanocomposite material is coated on ITO to construct an electrochemical sensor for the reliable detection of single-strand DNA (*t*DNA) which is cleaved from the genomic DNA of *Escherichia coli*. Under optimized conditions, linear detection of genomic DNA (*t*DNA) with concentration ranging from 1.3×10^{-12} to 1.3×10^{-23} M is observed and it is repeatable with a 1.3×10^{-23} M lowest level detection limit. The present modified electrode of PPyCB&H/GNS may show utility for constructing highly sensitive electrochemical sensors for the detection of *E. coli*.

Keywords Conducting polymer · Bioelectrode · *E. coli* · Polymer nanocomposites · Graphene nanosheets · DNA sensor

Introduction

Recently, several conducting polymers such as polypyrrole and its derivatives have drawn the attention of researchers because of its properties like high electrical conductivity, environmental stability, and comparative ease of synthesis and redox reversibility. These properties of polypyrrole derivatives make it suitable to be applied in the areas of secondary batteries, electrocatalysis, electrochromic electronic device, light-emitting devices, chemical sensors, and biosensors [1–5]. However, polypyrrole and other conducting electroactive polymers are constrained in practical use due to their fragility and insolubility which give rise to processing difficulties [6, 7]. Several approaches have been taken to improve the processability of conjugated polymers [8–11]. One possible approach is to introduce flexible polymeric matrices into the conducting rigid polymer. [12–14]. This is made possible with the help of flexible segments. Copolymerization is a desirable route than physical blending, which may lead to phase separation; the chemical linkage between the flexible matrix and the conjugated polymer enhances the solubility and processability [15, 16]. The polypyrrole copolymers with new structural architecture display different properties from polypyrrole homopolymer which may increase the application of conducting polymer. Several kinds of copolymers containing pyrrole and other insulating units, such as styrene, tetrahydrofuran, methyl methacrylate, and acryloyl chloride, have been studied [17–19]. All the above methods show enhanced mechanical and physical properties of polypyrrole. However, the synthesis of polypyrrole copolymer involves many

✉ Kannaiyan Dinakaran
kdinakaran.tvu@gmail.com

✉ R Sureshkumar
sukur74@yahoo.com

1   Department of Chemistry, Thiruvalluvar University, Vellore 632 115, India

2   Department of Chemical Engineering, Sri SivasubramaniyaNadar College of Engineering, Old Mahabalipuram Rd, OMR, Kalavakkam, 603110, Tamil Nadu, Chennai, India

3   Department of Polymer Science, University of Madras, Guindy Campus, Chennai 600 025, India

4   Department of Chemistry, R.V.Govt Arts College, Changalpattu 632101, India

steps and reaction conditions with diminished electrical conductivity leading to limited availability of copolymers for electrochemical studies. A simple and alternate technique is the immediate electrochemical copolymerization of monomers present in the mixture in an appropriate solvent [20–22]. Montmorillonite clay which is known as Maghnite-H + (Mag-H +), a nontoxic cationic, is used as a catalyst for cationic polymerization for a variety of vinylic and heterocyclic monomers [23–26]. However, using Maghnite-H + is expensive; hence, in this research work, para toluene sulfonic acid (*p*-TSA) is employed as a catalyst for the oxidative polymerization of pyrrole, 4-chlorobenzaldehyde, and hepataldehyde. The synthesized conducting polymer with graphene nanosheets is utilized to fabricate electrochemical sensing of DNA, particularly for the genomic DNA of *Escherichia coli* O157: H7.

In recent days, the major causes of illness and death across the globe is due to foodborne pathogens like *Escherichia coli* O157: H7, a commonly found bacterium in food and water. *E. coli* is a predominant species of facultative anaerobe in the gut of animals which is also found in soil, the intestinal tract of animals, fecal matter, marine, and estuarine water. *E. coli* imports profound effects on mammals [27]. *E. coli* O157: H7 is one of the most dreadful bacterium. Nowadays, a few colonies of *E. coli* O157:H7 is enough to cause severe illness, such as hemorrhagic colitis, hemolytic uremic syndrome, and fever particularly among children [28, 29]. Recently, a variety of novel detection techniques have been brought into under the light of real-time detection, showing enhanced sensitivity and reproducibility. These techniques have been made portable [30]. As far as electrochemical systems are concerned, traditional immunochemical procedures exhibit high specificity and sensitivity. Besides, the important steps are immobilization of *p*DNA onto the electrode surface and selection of a suitable electrode for the designing of an electrochemical immunosensor [31]. Conducting polymers (CP) are widely used as sensing platforms for the fabrication of practical interfaces and sensing surfaces. They combine properties of metallic and non-metallic compounds and make it a reasonable material for different application such as power devices [32], artificial muscles [33], biomedical engineering [34], chemosensors [35], biosensors [36] and surfaces for cell stimulation [37], and tissue designing and microorganism differentiation [38]. For instance, Filiz Kuralay et al. have studied the polypyrrole/multi-walled carbon nanotube modified graphite electrodes for the detection of (DNA) and polypyrrole/MWCNT electrodes exhibited a lowest detection limit of 1.55×10^{-8} [39]; polypyrrole-dendrimer hybrids also studied for the mRNA detection [40] poly(3,4-ethylenedioxythiophene) (PEDOT)-coated chitosan as electrode to study the DNA-drug interaction [41]. Hydroxyl and carboxyl functionalized GNS are used to fabricate DNA sensors with high sensitivity

due to their excellent electrical properties as well as conductivity [42]. Zinc oxide nanorods and graphene nanoflake composite functionalized with *ss*DNA towards the development of impedimetric biosensor show the lowest detection limit range of 10^{-16} M to 10^{-6} M [43]. Filiz Kuralay et al. reported a lowest detection limit of 1.25 mg L^{-1} for double-stranded DNA using a titanium dioxide–coated graphene-based nanocomposite electrode [44]. Ida Tiwari et al. reported the lowest detection limit of 1×10^{-16} M [45] using graphene oxide/chitosan composite decorated with nickel ferrite nanoparticle-based biosensing for *E. coli* through DPV method. In this work, we have proposed a new electrochemical sensing platform (PPyCB&H/GNS) with an excellent electrical activity that is used to fabricate a genosensor by immobilizing probe sequence specific to *E. coli* and incorporating target genomic *ss*DNA. The hybridization between *E. coli* *p*DNA and *t*DNA on PPyCB&H/GNS modified electrode is detected with DPV measurement. The approach is further employed to determine the concentration of *E. coli*. By far, this is the first work that shows the application of PPyCB&H/GNS nanocomposite for the fabrication of electrochemical DNA biosensor for rapid detection of *E. coli* with high sensitivity and selectivity.

Experimental sections

Materials and methods

Pyrrole, 4-chlorobenzaldehyde, heptaldehyde, para toluene sulfonic acid (*p*-TSA), sodium chloride (NaCl), potassium chloride (KCl), disodium hydrogen phosphate (Na$_2$HPO$_4$), and potassium dihydrogen phosphate (KH$_2$PO$_4$) are of analytical grade and purchased from SRL, Fischer Scientific and Sigma-Aldrich. They are used directly without further purification. All glassware are cleaned successively with aquaregia and Deionized water and then dried before use. Probe DNA (*p*DNA): amine-50-GGT CCG CTT GCT CTC GC-30 and Target DNA (*t*DNA): genomic DNA are purchased from Synergy Scientific products (India). Oligonucleotide solution is prepared in Phosphate buffer of pH 7.0 and stored at -20 °C before use. (Scheme 1)

Synthesis of PPyCB&H copolymer

In a 100-mL beaker, distilled pyrrole (2 mmol), 4-chloro benzaldehyde (2 mmol), and heptaldehyde (2 mmol) are dissolved in 20 mL of chloroform and 0.5 g of *p*-toluene sulfonic acid (*p*-TSA) is added. The mixture is placed in a microwave oven to be irradiated at full power for 30 min. At the end of the reaction, the resulting mixture is filtered to remove the impurities and then slowly added to methanol with stirring, and then, the polymer is dried under vacuum at

Scheme 1 Synthesis of ter-polymer

Poly[(Pyrrole-2,5-diyl)-co (benzylidene) and (heptaldehyde)] (PPyCB&H)
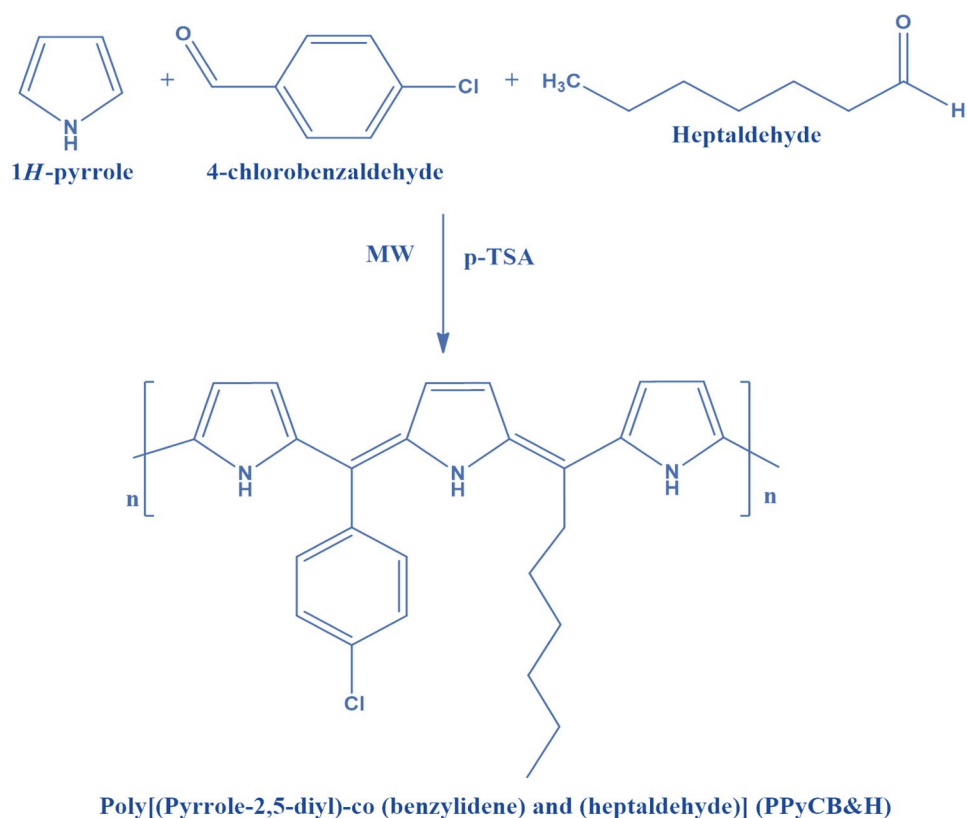
room temperature for 24 h. Further, the catalyst is separated from the common base and water.

Synthesis of graphene nanosheet

Metallic copper powder (10 g, 99.7% pure) and $CHCl_3$ (25 mL) are heated to 200 °C for 10 h in a Teflon lined stainless steel autoclave with 55 mL capacity. After the reaction, the autoclave is cooled to room temperature. The resulting solid is filtered carefully, and the mother liquor is collected for further analysis. And then, the product is treated with 6 M HNO_3 solution at room temperature for 12 h, followed by filtration and washed with distilled water several times until the filtrate attains a neutral P^H and is chlorine free. Finally, the solid mass is air-dried at 100 °C for 10 h. The final yield of the carbon product is approximately 0.9 g.

Preparation of PPyCB&H/GNS nanocomposite

A total of 1 mg GNS is dispersed in 10 mL tetrahydrofuran (THF) and ultrasonicated for 1 h to get a suspension. Further, 1 g of PPyCB&H is added in the THF solution followed by ultrasonication for 30 min which results in (PPyCB&H/GNS) in the formation of nanocomposite.

Modification of PPyCB&H/GNS nanocomposite onto ITO electrode

The bare ITO is polished carefully with 0.5 and 0.03 μm alumina slurry and cleaned successively with ethanol and double-distilled deionized water by sonication. It is finally dried in N_2 stream. ITO plates are standardized by measuring conductivity of bare ITO sheets using a multimeter. The ITO-coated glass sheet should have a specified surface resistivity in the range of 10 ohms/sq. to 100 ohms per square. After cleaning, 1.0 mg of PPyCB&H/GNS is ultrasonically dispersed into 1.0 mL THF to form a homogeneous solution. A total of 5.0 μLPPyCB&H/GNS solution is placed onto the ITO surface and dried. The obtained PPyCB&H/GNS modified electrode is stored in air at room temperature.

Fabrication of nucleic acid-functionalized PPyCB&H/GNS/pDNA ITO electrode

Exactly 20 mL of *p*DNA is immobilized on the PPyCB&H/GNS/ITO electrode surface, via oligonucleotide which can be used for binding with graphene through van der waals forces, π-π stacking, and/or hydrogen bond [46]. Hybridization is performed by incubating the prepared PPyCB&H/

Fig. 1 FTIR spectrum of GNS PPyCB&H and PPyCB&H/GNS
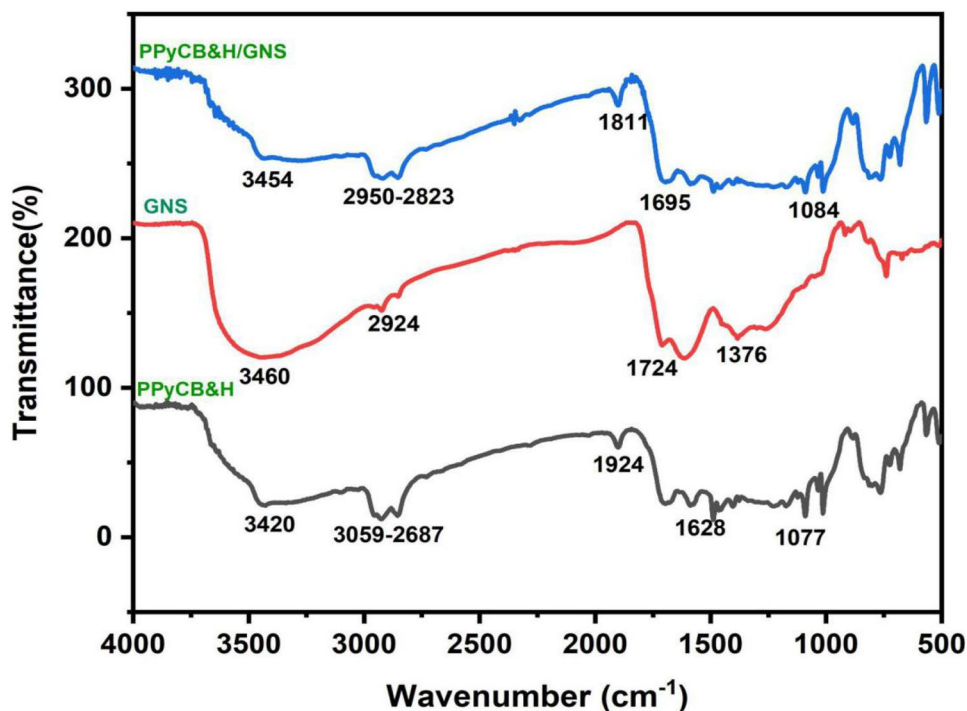
GNS/ITO bioelectrodes in the various concentration of target DNA solution for 30 min in PBS medium, and the corresponding change in current is measured by DPV.

Results and discussion

The conjugated terpolymer based on pyrrole has been synthesized using p-toluenesulfonic acid as catalyst. The synthesized polymer was characterized by FTIR and NMR spectroscopy.

Spectral studies

The polymer nanocomposites prepared from PPyCB&H/GNS is analyzed using FT-IR spectra. Figure 1 shows the FT-IR spectra of GNS, PPyCB&H, and PPyCB&H/GNS. The peak at 3420 cm^{-1} is due to the vibration of N–H in pyrrole, the peak at 3059–2687 cm^{-1} is due to the aromatic C-H stretching in 4-chloro benzaldehyde, the peak at 1924 cm^{-1} corresponds to the aromatic C-H bending in 4-chloro benzaldehyde, the peak at 1445 cm^{-1} is attributed to the aliphatic C-H stretching in heptaldehyde, the peak at 1317 cm^{-1} is due to the aliphatic C-H bending, the vibration of the phenylene conjugated C=C in pyrrole ring appeared at 1628 cm^{-1}, and aromatic C=C stretching peak of pyrrole ring and 4-chloro benzaldehyde appeared at 1596 cm^{-1}. The aromatic C-N stretching peak that appears at 1148 cm^{-1} and halogen stretching peak that appears at 748 cm^{-1} correspond

to C–Cl bond in 4-chlorobenzaldehyde. GNS, the peaks that correspond to C=O stretching, appears at 1724 cm^{-1}, C–O–C stretching at 1376 cm^{-1}, and the broadband observes at ~3253 cm^{-1} is due to the hydroxyl group (-OH) stretching. Interestingly, the band at 3454 cm^{-1} is slightly shifted, the peak attributes to the aromatic C-H stretching slightly shifted to 2950–2823 cm^{-1}, and after the functionalization of PPyCB&H/GNS, the C=O group is shifted to 1695 cm^{-1} which confirms the formation PPyCB&H/GNS polymer nanocomposites.

^{1}H-NMR spectrum of poly [(pyrrole-2, 5-diyl)-co-(benzylidene) and (heptaldehyde)] is shown in Fig. 2, which indicates the characteristic of aliphatic hydrogen resonance at about (e) 1.18 to 2.93 ppm in multiple signals; the aromatic protons of pyrrole ring (a) appears at 6.37 ppm, the aromatic protons of 4-chlorobenzaldehyde (d) proton appears at 7.46 to 7.44 ppm then conjugates the neighboring protons (c) which appears at 7.48 to 7.79 ppm and the NH- protons of polypyrrole (b) which appears at 9.28 ppm as a singlet.

Morphological studies

Figure 3 displays the XRD patterns of GNS, PPyCB&H, and PPyCB&H/GNS. As it can be seen in the case of GNS, the diffraction peak centered at $2\theta = 24.8°$ corresponding to (002) plane which indicates the monolayer structure of GNS. Moreover, in case of pure conducting polymer PPyCB&H, a broad peak is found at $2\theta = 19.5°$ representing the

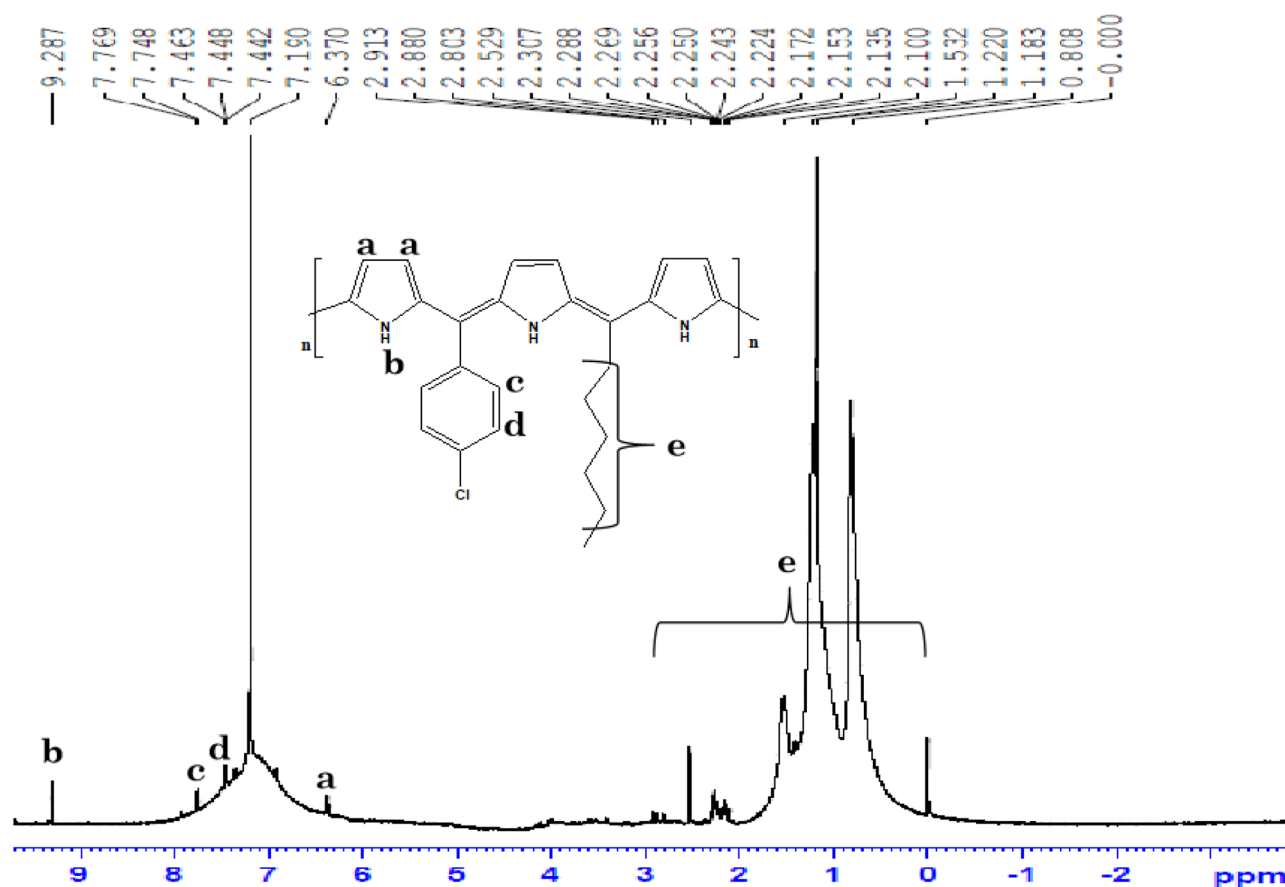**Fig. 2** ^{1}H-NMR spectrum of poly[(pyrrole-2,5-diyl)-co-(benzylidene) and (heptaldehyde)] (PPyCB&H)

characteristic peak of amorphous structure, and the peak is shifted to $2\theta = 21.2°$ for the prepared PPyCB&H/GNS composite. This suggests that PPyCB&H and GNS are blended well to form PPyCB&H/GNS, while the π-π stacking interaction between PPyCB&H chains and GNSnanosheets is responsible for the diffraction peak shift. Figure 3b represents the Raman spectra of GNS. The Raman spectra of GNS displayed intense bands corresponding to G-band at 1580 cm^{-1} and the D-band at 1350 cm^{-1} credited to the E2g vibrational mode of sp2 hybridized C–C and A1g mode in the disordered edge region of the nanosheets, respectively.

The morphology of the pristine components and the composite samples are analyzed with scanning electron microscopy. Figure 4a–d represent a typical FESEM image of GNS and PPyCB&H/GNS. The images show (Fig. 4a–b) more sheet structure of graphene. In Fig. 4c–d, sheet layers of GNS are wrapped by the polymer matrix; see that the morphology to PPyCB&H/GNS in white line corresponds to the GNS and red line corresponded to the PPyCB&H indicating the formation of a graphene sheet coating of PPyCB&H on the surface of the GNS. The TEM images of GNS are presented in Fig. 5a–c. The TEM images indicate that the samples are in nanosheet-like structure with a smooth surface. It is observed that nanosheets are ultra-thin and highly transparent, crumpled with folds at edges.

Electrochemical studies

Cyclic voltometry

The cyclic voltammetry curves of the GNS, PPyCB&H, PPyCB&H/GNS, and PPyCB&H/GNS/*ss*DNA recorded in the presence of 0.1 M of PBS solution at a scan rate of 100 mV/s are represented in Fig. 6. The electrode modified with PPyCB&H composite shows a slightly lower redox peak which may be due to inhibition of electron transfer. The GNS exhibited good redox peak potential when compared with PPyCB&H, and the oxidation potential of GNS appeared at -0.4 V, and the corresponding reduction potential appeared at 0.52 V. However, the nanocomposite PPyCB&H/GNS electrode is found to have high redox peak which may be due to the fact that the intrinsic conductivity of GNS may aid the electron transfer to PPyCB&H composite leading to superior conductivity. The immobilization of *ss*DNA slightly increases the oxidation and reduction potential.

Fig. 3 (**a**) XRD studies of GNS, PPyCB&H, and PPyCB&H/ GNS nanocomposites and (**b**) Raman studies of GNS
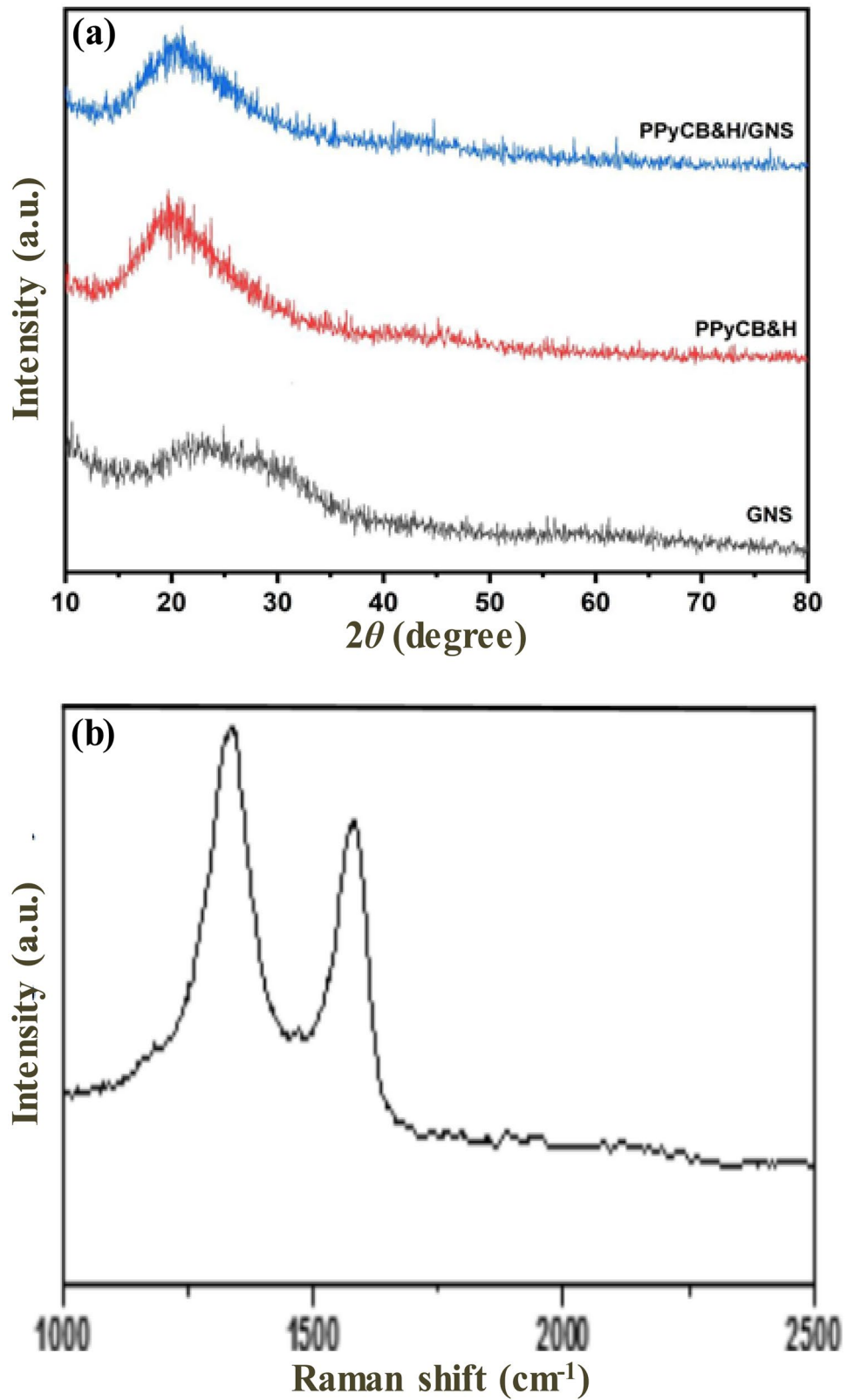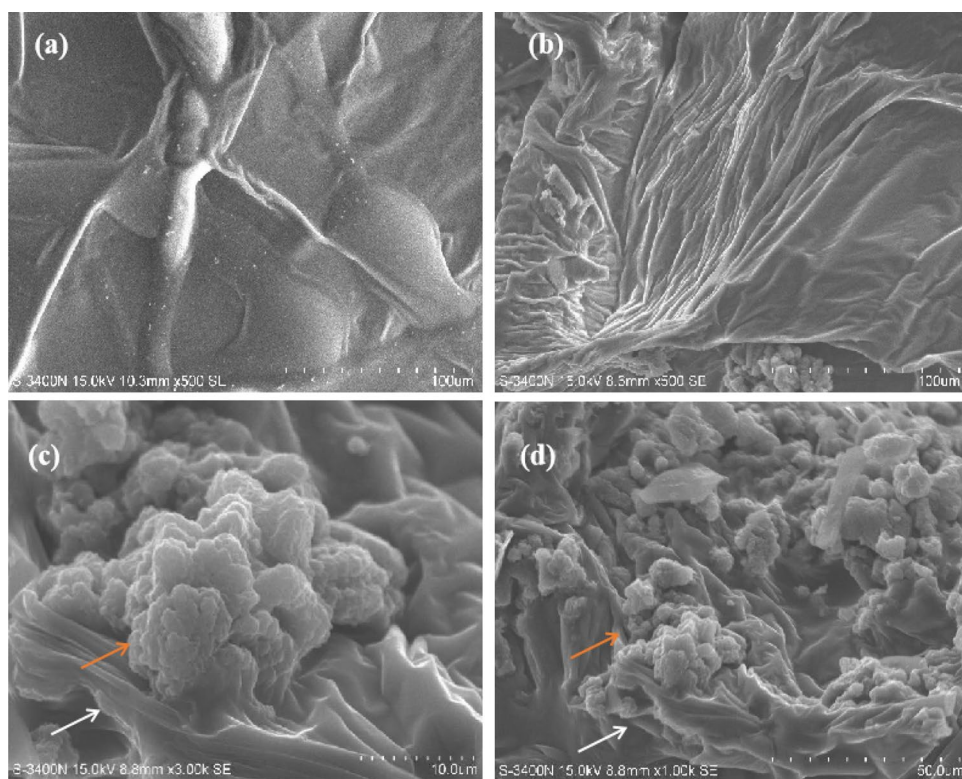
Fig. 4 SEM images of synthesized GNS and PPyCB&H/GNS composite

EIS and Bode plot studies

EIS is employed to characterize the interface properties of the modified electrodes. In EIS measurement shown in Fig. 7, the semicircle diameter at higher frequencies in the Nyquist diagram of impedance spectroscopy equals the interfacial electron transfer resistance (Ret), which controls the electron transfer of the redox probe at the electrode surface. Figure 8a shows Nyquist diagrams of 0.1 M PBS at different electrodes. The electron transfer resistance (Ret) of PPyCB&H electrode is very large as compared to that of the GNS modified electrode due to the enhanced conductivity and electrochemical activity of composites film. The composites of PPyCB&H/GNS have less resistance value and good electrical conductivity. The electrode is immobilized with pDNA, and the electron transfer resistance value decreases due to the reason that the immobilized DNA generates a large number of negative charge which could interact with the polymer nanocomposite, resulting in the enhanced conductivity of the electrode. The change in the phase angle in the Bode plot is chosen as a prominent EIS element in the frequency region of 0–40,000 Hz as shown in
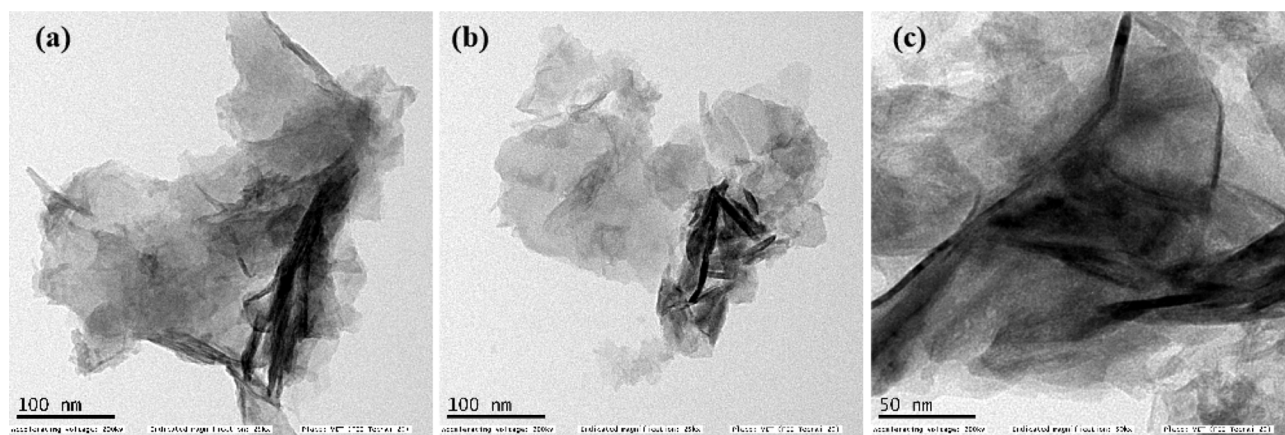

Fig. 5 TEM images of synthesized graphene nanosheets (GNS)

Fig. 6 Cyclic voltometry of GNS, PPyCB&H, PPyCB&H/GNS, and PPyCB&H/GNS/*ss*DNA
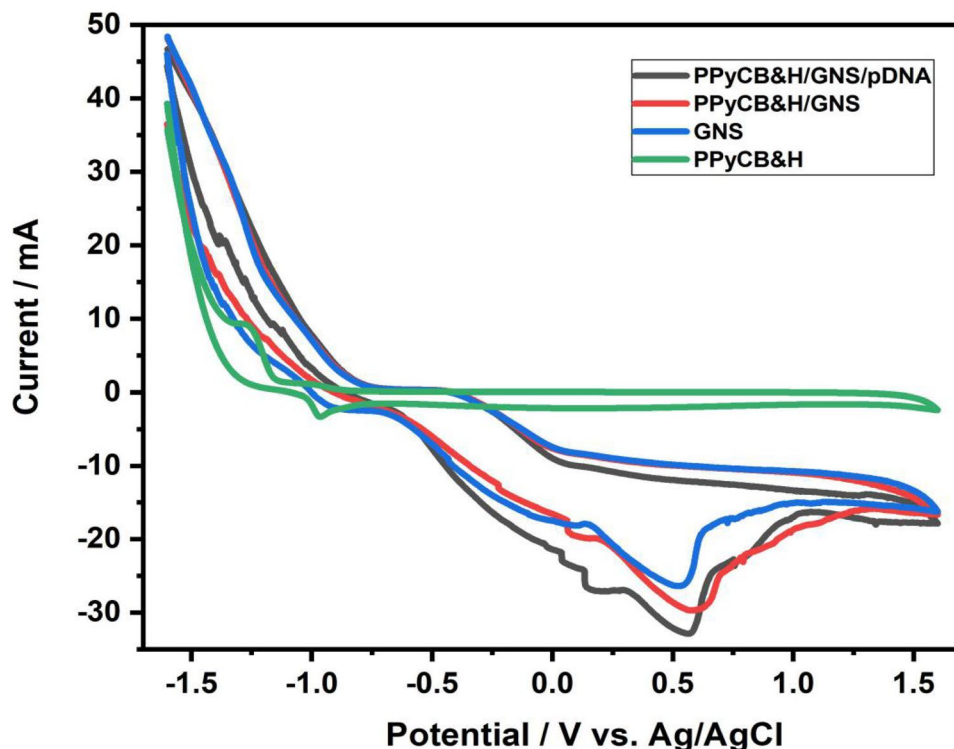

Fig. 8b. The PPyCB&H electrode shows the phase angle at 67.19° at ~2 Hz. These phase angle of the GNS PPyCB&H/GNS and PPyCB/GNS/*p*DNA is shifted to 48°, 46.3°, and 43.4° at a lower frequency of ~1 Hz.

Scan rate

Cyclic voltammetry is performed with the modified PPyCB&H/GNS/ITO electrode at various scan rates in the range 10–100 mV s^{-1} and presented in Fig. 8a–b. It is observed from Fig. 8a that increase in scan rate results in the increase of anodic peak current (Ipa) and cathodic peak current (Ipc). It is due to the reason that the high electrical charged PPyCB&H/GNS promotes the electron transfer to the analyte solution. Figure 8b describes the plot of peak currents (Ip) as a function of the square root of scan rate which exhibits linear behavior which further increases linearly as a function of scan rate for
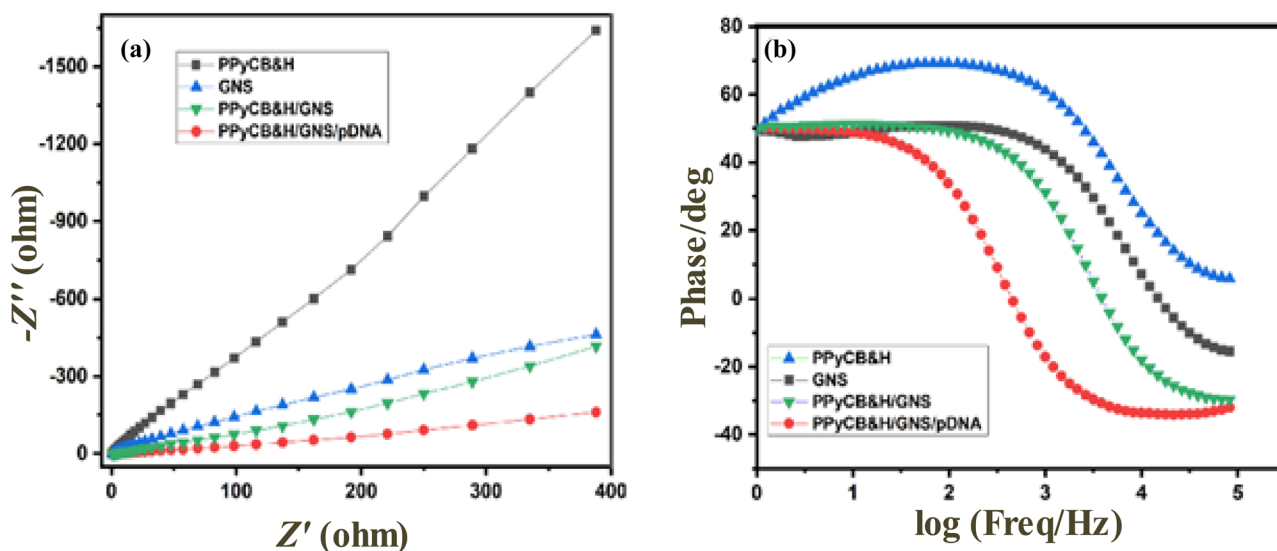

Fig. 7 (**a**) EIS and (**b**) Bode plots of GNS, PPyCB&H, PPyCB&H/GNS, and PPyCB&H/GNS/*p*DNA
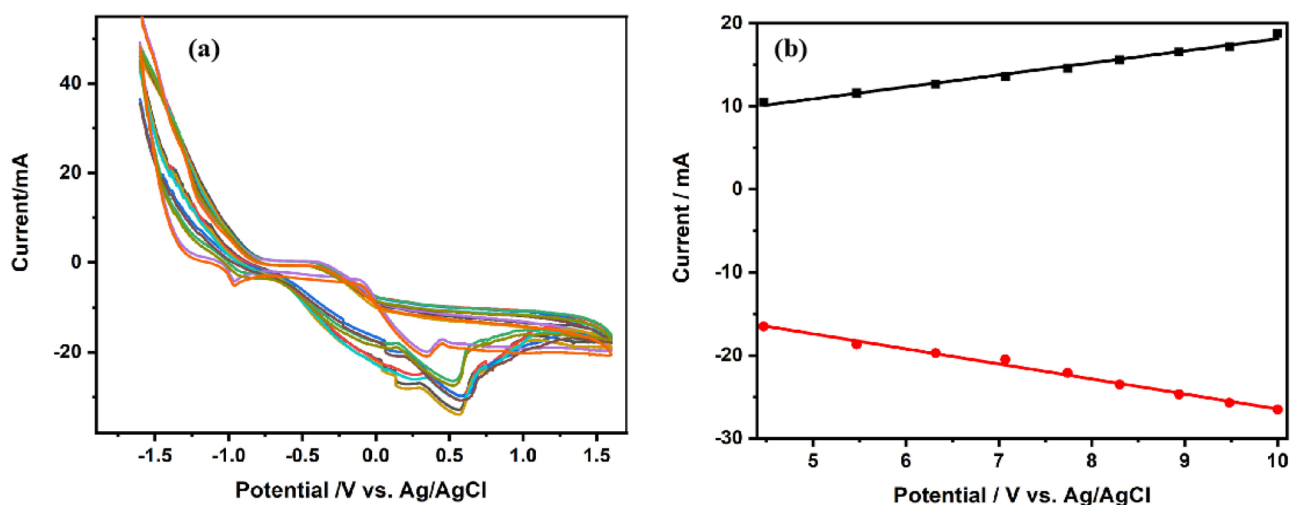
Fig. 8 Cyclic voltammetric variation of (**a**) PPyCB&H/GNS/ITO electrode with scan rate in PBS 0.1 M, pH 7.4. (**b**) The variation of current with square root of scan rate

PPyCB&H/GNS/ITO bioelectrode. Based on the above result, it can be concluded that the prepared bioelectrode has good electron transfer due to the synergistic effect of large surface area and conductivity of graphene and PPyCB&H nanocomposites.

DPV response of various electrodes

The electrochemical responses of pDNA of *E. coli* for a 100 μL in PBS (pH = 5.0) using PPyCB&H/ITO, GNS/ITO, and PPyCB&H/GNS/ITO electrodes are investigated through DPV. As shown in Fig. 9a, a small oxidation peak is observed at the bare ITO. GNS-coated ITO electrode

shows a significant increase in oxidation peak current. As observed from the figure, the oxidation peak current is further enhanced for the composite PPyCB&H/GNS/ITO electrode. The GNS and PPyCB&H hybrid system promotes the electron transfer between the solution and electrode surface due to the synergistic amplification effect of GNS with PPyCB&H. The comparison of the various modified electrode with their DPV responses are plotted as a bar diagram in Fig. 9b, which clearly indicates the enhanced response from the PPyCB&H/GNS/ITO electrode in Fig. 9. The specificity of the electrode setup has been conducted by hybridizing tDNA of other pathogens and found that there is no change in peak current of the DPV analysis.

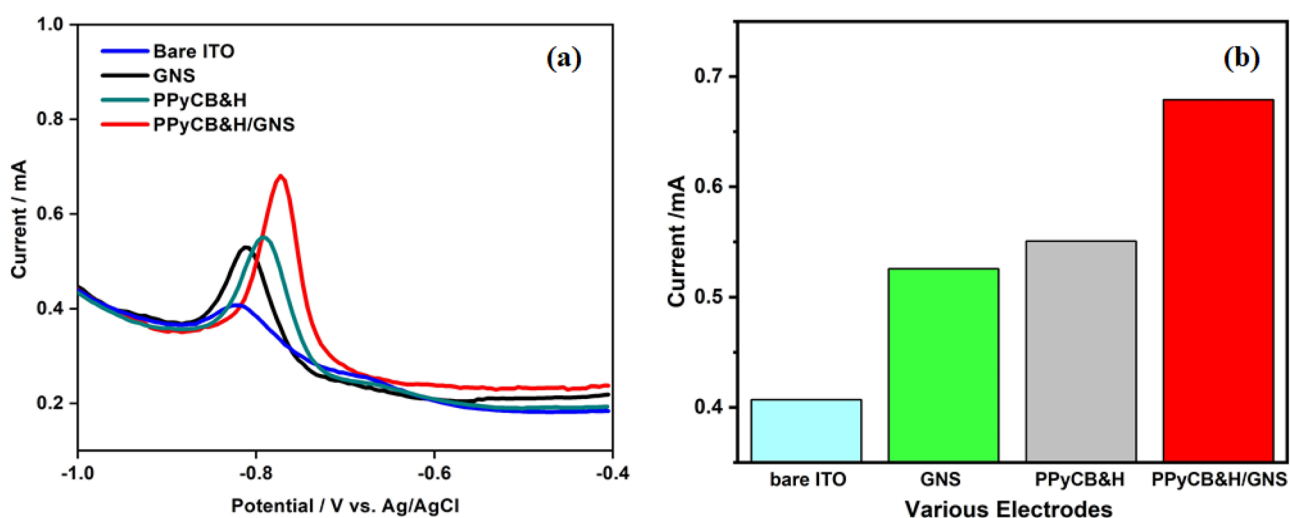

Fig. 9 Electrochemical properties of the fabricated electrodes. The DPV studies of various electrode in (**a**) bare ITO, GNS, PPyCB&H, and PPyCB&H/GNS in 0.1 M PBS (pH 7.0) at 100 mV s^{-1} scan rate. (**b**) Sensitivity of the electrodes
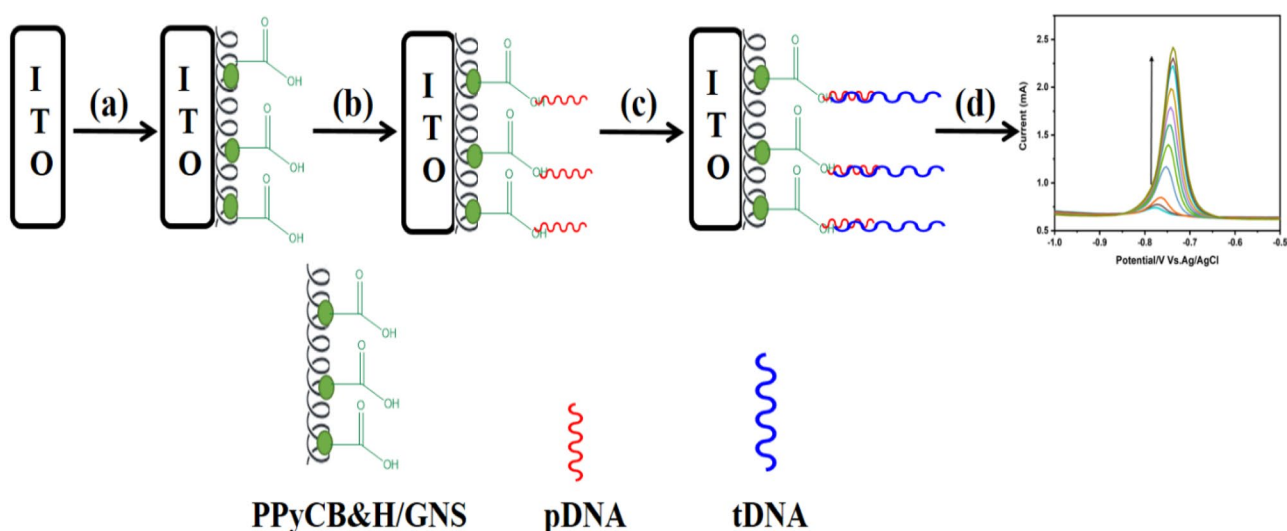
Fig. 10 A schematic diagram of the modification process of ITO. (**a**) Spin coating of PPyCB&H/GNS on ITO, (**b**) PPyCB&H/GNS/ITO modified with *p*DNA, (**c**) PPyCB&H/GNS/*p*DNA incubate with the *t*DNA, and (**d**) detection technique of DPV

Sensor test

The detection procedure for the detection of single strand genomic DNA of *E. coli*, *t*DNA, using the oligonucleotide modified PPyCB&H/GNS/ITO electrode, is presented schematically in Fig. 10. The electrochemical detection ability of the PPyCB&H/GNS polymer nanocomposite is studied by exposing the oligonucleotide modified PPyCB&H/GNS/ITO electrode to the *t*DNA of *E. coli* within the wide concentration range of 1.3×10^{-12} to 1.3×10^{-23} M. The sensing studies are repeated three times with three different ITO slides, and there is not much difference in the results obtained in all the three slides. Figure 11a shows an increase in current density with increasing concentrations of *t*DNA. The response of GNS and PPyCB&H/GNS on ITO is determined by the DPV studies at 0.01 mVs^{-1} scan rate. The largest oxidation peak of the PPyCB&H/GNS nanocomposite electrode has obtained the potential of -0.7 V due to high electron transfer ability and electrical conductivity. After incubation of *t*DNA, a larger increase in oxidation current density of *t*DNA/PPyCB&H/GNS/ITO is seen in the voltammogram. This is due to the charge transfer as a result of enhanced electron transfer and the binding of *t*DNA on the PPyCB&H/GNS surface. In the presence of *t*DNA, the oxidation peak current increases proportionally with the concentration of genomic DNA. When the pathogenic *t*DNA concentration increases, the current density also increases due to the kinetics of interfacial electron-transfer and decrease in the electron-transfer resistance from the medium to the
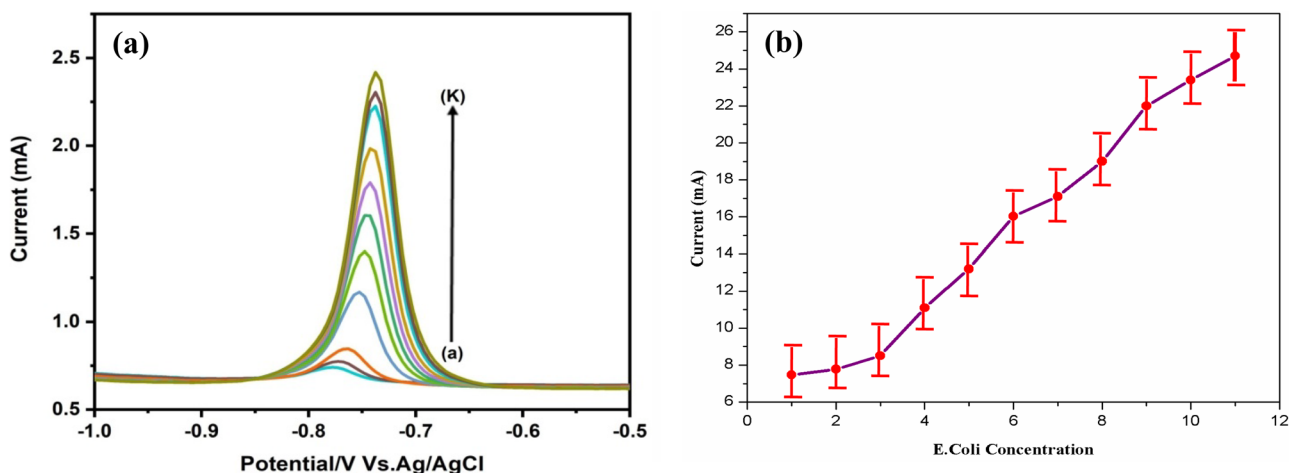

Fig. 11 (**a**) DPV response of *p*DNA/PPyCB&H/GNS/ITO bioelectrode as a function of *t*DNA concentration (1.3×10^{-12} to 1.3×10^{-23} M) in PBS solution (pH 7) and (**b**) plot of the DPV response of *t*DNA/PPyCB&H/GNS/ITO bioelectrode vs. the concentration of *E. coli*

Table 1 Comparison of different electrodes for the electrochemical determination of pathogens involving DNA hybridization

Materials	Methods	Linearity range (concentration)	Detection limit	References
GO-GNP/PPY/ITO	DPV	$1\times10^{-}$–1×10^{-15} M	1×10^{-15} M	[47]
PPY-Ag	LSV	3.0×10^{-4}–5.0×10^{-4} μM	5.0×10^{-4} μM	[48]
2,5bis(2-Thienyl)-N-(3-Phosphorylpropyl) Pyrrole	CV/LSV	1.8×10^{-12}–1.8×10^{-21} M	1.8×10^{-21} nM	[49]
PPy/MWCNTs	CV/EIS	1.0×10^{-6}–1.0×10^{-11} nM	1.0×10^{-11} nM	[50]
PPy-Polyaniline-Au	EIS	1.0×10^{-6}–1.0×10^{-13} M	1.0×10^{-13} M	[51]
PPy-Poly(3,4-ethylenedioxythiophene)-Ag	EIS	1.0×10^{-11}–1.0×10^{-14} M	1.0×10^{-14} M	[52]
PPyCB&H/GNS	DPV	1.3×10^{-12}–1.3×10^{-23} M	1.3×10^{-23} M	Present work

Fig. 12 Stability of the DNA biosensor under successive CV scans for 20 cycles after incubating with 1.3×10^{-12} M tDNA
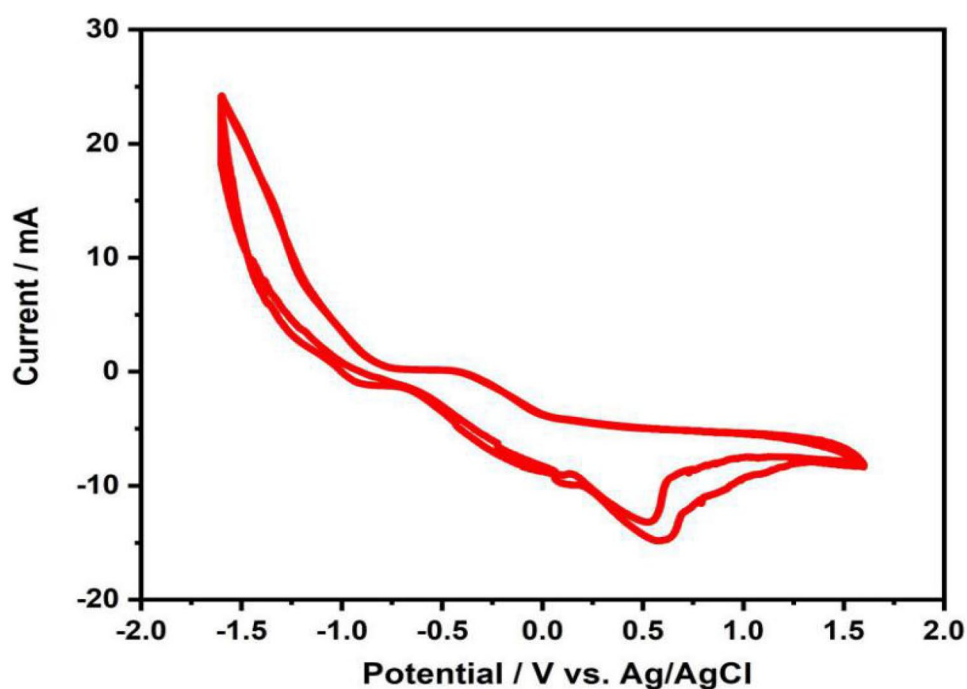
electrode's surface. The plot of current density vs. the logarithm of the concentration of *E. coli* as shown in Fig. 11b indicates a linear relationship with a correlation coefficient of 0.9859. The limit of detection of this sensor is found to be 1.3×10^{-12} to 1.3×10^{-23} M, the lowest detection limits are 1.3×10^{-23} M. The electrochemical detection of DNA using various polypyrrole nanocomposite materials are tabulated in Table 1 and in Fig. 11.

Reliability and stability properties of the biosensor

Under the experimental conditions, the electrochemical reproducibility and stability of PPyCB&H/GNS polymer nanocomposite (Fig. 12) are analyzed by continual

20 cycling procedure. The redox curves indicate that the change is insignificant with respect to peak current. In addition, pDNA/PPyCB&H/GNS/ITO are stored for 20 days in distilled water at 4 °C and the reduced current displayed excellent stability. The slight decrease in signal is noted at 10 days, and therefore, the biosensor has good storage stability.

Conclusion

In summary, an electrochemical biosensor PPyCB&H/GNS/pDNA polymer nanocomposite for the detection of *E. coli* is successfully developed. The polymer nanocomposite and the probe DNA immobilized PPyCB&H/GNS are

characterized by physicochemical methods to show the dispersion of GNS in PPyCB&H. The fabricated *p*DNA/PPyCB&H/GNS/ITO working electrode demonstrated sensitivity current peaks for *E. coli t*DNA proportional to the concentration ranging from 1.3×10^{-12} to 1.3×10^{-23} M with a LOD value of 1.3×10^{-23} M. The overall results indicate that PPyCB&H/GNS polymer nanocomposite exhibits good electrochemical activity which attributes to the presence of graphene nanosheets and synergistically improves electron transfer. Moreover, the conducting polymer provides a large specific surface area for pathogen immobilization and aids the conducting network formation. Thus, the designed *p*DNA/PPyCB&H/GNS/ITO demonstrate sensitivity for pathogen detection.

References

1. Mermilliod N, Tanguy J, Petiot F (1986) A study of chemically synthesized polypyrrole as electrode material for battery applications. J Electrochemi Soc 133:1073–1079

2. MacDiarmid AG, Epstein AJ (1997) Application of thin films of polyaniline and polypyrrole in novel light emitting devices and liquid-crystal devices. ACS Symp Series 672:395–407

3. Mao HY, Pickup PG (1989) Electronically conductive anion-exchange polymers based on polypyrrole preparation, characterization, electrostatic binding of ferrocyanide and electrocatalysis of ascorbic-acid oxidation. J Electroanal Chem Interfa Electrochem 265:127–142

4. Ramanavicius A, Ramanaviciene A, Malinauskas A (2006) Electrochemical sensors based on conducting polymer-polypyrrole. Electrochim Acta 51:6025–6037

5. Xue HG, Mu SL (1995) Bioelectrochemical response of the polypyrrole xanthine-oxidase electrode. J Electroanal Chem 397:241–247

6. Lindenberger H, Schafer-Siebert D, Roth S, Hanack M (1987) Synthesis and properties of polypyrrole prepared by electrochemical polymerization of alpha-bipyrrole. Synthet Metals 18:37–41

7. Qian RY, Qiu JJ, Shen DY (1987) Conducting polypyrrole electrochemically prepared from aqueous-solutions. Synthet Metals 18:13–18

8. De Paoli MA, Gazotti WA (2002) Conductive polymer blends: preparation, properties and applications. Macromole Symp 189:83–103

9. Li YF, Ouyang JY (2000) Effect of nonionic surfactant additives on the electro-polymerization of pyrrole in aqueous solutions. Synthet Metals 113:23–28

10. Corres MA, Mulgica A, Carrasco PM, Cortazar MM (2006) Effect of crystallization on morphology-conductivity relationship in polypyrrole/poly(epsiloncaprolactone)blends. Polymer 47:6759–6764

11. Balci N, Toppare L, Akbulut U, Stanke D, Hallensleben ML (1998) Polypyrrole grafts synthesized via electrochemical polymerization. J Macromole Sci Pure Appl Chem 35:1727–1739

12. Lee Y, Shin D, Cho J, Park YH, Son Y, Baik DH (1998) Ionic interactions in polyacrylonitrile/polypyrrole conducting polymer composite. J Appl Polym Sci 69:2641–2648

13. Levine KL, Iroh JO (2004) Resistance of the polypyrrole/polyimide composite by electrochemical impedance spectroscopy. J Porous Mater 11:87–95

14. Yin WS, Yan TJ, Gan LM, Chew CH, Liu HW, Gan LH (1998) Conductive composite films based on polypyrrole and crosslinkedpoly(styrene butylacrylateacrylic acid). Euro Polym J 34:1763–1766

15. Mano V, Felisberti MI, Matencio T, DePaoli MA (1996) Thermal, mechanical and electrochemical behavior of poly (vinyl chloride)/polypyrrole blends(PVC/PPy). Polymer 37:5165–5170

16. Brahim S, Guiseppi-Elie A (2005) Electroconductive hydrogels: electrical and electrochemical properties of polypyrrole-poly(HEMA) composites. Electro anal 17:556–570

17. Park YH, Kim KW, Jo WH (2002) Preparation and characterization of conducting poly(acryloyl chloride)-g-polypyrrole copolymer. Polym Adv Technol 13:670–677

18. Tarkuc S, Sahin E, Toppare L, Colak D, Cianga I, Yagci Y (2006) Synthesis, characterization and electrochromic properties of a conducting copolymer of pyrrole functionalized polystyrene with pyrrole. Polymer 47:2001–2009

19. Kizilyar N, Toppare L, Onen A, Yagci Y (1999) Synthesis of conducting PPy/pTHF copolymers. J Appl Polym Sci 71:713–720

20. Borole DD, Kapadi UR, Mahulikar PP, Hundiwale DG (2006) Electrochemical synthesis and characterization of conducting copolymer: Poly (o-aniline-co-o-toluidine). Mater Lett 60:2447–2452

21. Mu SL (2006) Poly(aniline-co-o-aminophenol) nanostructured network: Electrochemical controllable synthesis and electrocatalysis. Electrochim Acta 51:3434–3440

22. Dhanalakshmi K, Saraswathi R (2001) Electrochemical preparation and characterization of conducting copolymers: poly(pyrrole-co-indole). J Mater Sci 36:4107–4115

23. Belbachir M, Bensaoula A (2001) Composition and method for catalysis using bentonites US patent 6,274,527, USA

24. Yahiaoui A, Belbachir M (2006) Ring-opening polymerization of styrene oxide with maghnite-H+ as ecocatalyst. J Appl Polym Sci 100:1681–1687

25. Hachemaoui A, Yahiaoui A, Belbachir M (2006) Synthesis and characterization of water soluble poly (Nacetyl)iminoethylene and poly (ethyleneimine) byion- exchanged clay montmorillonite. J Appl Polym Sci 102:3741–3750

26. Meghabar R, Megherbi A, Belbachir M (2003) Maghnite-H+, and cocatalyst for cationic polymerization of N-vinyl-pyrrolidone. Polymer 44:4097–4100

27. Dou WC, Tang WL, Zhao GY (2013) A disposable electrochemical immunosensor arrays using 4-channel screen-printed carbon electrode for simultaneous detection of Escherichia coli O157:H7 and Enterobacter sakazakii. Electrochim Acta 97:79–85

28. Zhang X, Geng P, Liu H, Teng Y, Liu Y, Wang Q, Zhang W, Jin L, Jiang L (2009) Development of an electrochemical immunoassay for rapid detection of E. coli using anodic stripping voltammetry based on Cu@Au nanoparticles as antibody labels. Biosens Bioelectron 24:2155–2159

29. Manges AR, Johnson JR (2012) Food borne origins of Escherichia coli causing extraintestinal infections. Clinic Infecti Dis 55:712–719

30. Yoon JY, Kim B (2012) Lab on a chip pathogen sensors for food safety. Sensors 12:10713–10741

31. Yang GJ, Huang JL, Meng WJ, Shen M, Jiao XA (2009) A reusable capacitive immunosensor for detection of Salmonella spp. based on grafted ethylene diamine and self-assembled gold nanoparticle monolayers. Anal Chim Acta 647:159–166

32. Inamuddin SKM, Kim SI, Insuk S, Kim SJ (2009) A conducting polymer/ferritin anode for biofuel cell applications. Electrochim Acta 54:3979–3983

33. Jage EWH, Smela E, Inganäs O (2000) Micro fabricating conjugated polymer actuators. Science 290:1540–1545

34. Guimard N, GNSmez K, Schmidt NEC, (2007) Conducting polymers in biomedical engineering. Prog Polym Sci 32:876–921

35. Pattananuwat P, Tagaya M, Kobayashi T (2015) A novel highly sensitive humidity sensor based on poly(pyrrole-co-formyl pyrrole) copolymer film: AC and DC impedance analysis. Sens Actuators B Chem 209:186–193

36. Li L, Wang Y, Pan L, Shi Y, Cheng W, Shi Y, Yu G (2015) A nanostructured conductive hydrogels based biosensor platform for human metabolite detection. Nano Lett 15:1146–1151

37. Svennersten K, Berggren M, Dahlforsa A, Jager EWH (2011) Mechanical stimulation of epithelial cells using polypyrrole microactuators. Lab Chip 11(19):3287–3293

38. Golabi M, Turner APF, Jager EWH (2016) Tunable conjugated polymers for bacterial differentiation. Sens Actuators B: Chem 222:839–848

39. Filiz K, Nilgün D (2020) Polypyrrole-based nano hybrid electrodes: their preparation and potential use for DNA recognition and paclitaxel quantification. Chem Select 5:4708–4714

40. Dongwei W, Jiasheng W (2021) A sensitive and label-free electrochemical microRNA biosensor based on polyamidoamine dendrimer functionalized polypyrrole nanowires hybrid. Mikrochim Acta 188:173

41. Filiz K, Serpil D, Melek K, Lutfi O, Aysegul Uygun O (2014) Poly(3,4-ethylenedioxythiophene) coated chitosan modified disposable electrodes for DNA and DNA-drug interaction sensing. Colloid Surf D: Biointerf 123:825–830

42. Singh A, Sinsinbar G, Choudhary M, Kumar V, Pasricha R, Verma HN, Singh HP, Arora K (2013) Graphene oxide-chitosan nanocomposite based electrochemical DNA biosensor for detection of typhoid. Sens Actuators B 185:675–684

43. Nandita J, Chandra NJ, Shipra MP, Solanki I, Tiwaril BD (2020) An impedimetric biosensor based on electrophoretically assembled ZnO nanorods and carboxylated graphene nanoflakes on an indium tin oxide electrode for detection of the DNA of Escherichia coli O157:H7 Microchim Acta 187:1

44. Filiz K, Selma T, Ferhat B, Lutfi O, Aysegul Uygun O (2016) Biosensing applications of titanium dioxide coated graphene modified disposable electrodes. Talanta 160:325–331

45. Tiwari I, Monali S, Pandey CM, Suman G (2015) Electrochemical detection of a pathogenic Escherichia coli specific DNA sequence based on a graphene oxide chitosan composite decorated with nickel ferrite nanoparticles. RSC Adv 5:67115–67124

46. Tang L, Wang Y, Liu Y, Li J (2011) DNA directed self-assembly of graphene oxide with applications to ultrasensitive oligonucleotide assay. ACS Nano 5:3187–3827

47. Tiwari I, Gupta M, Mouli Pandey C, Mishra V (2015) Gold nanoparticles decorated graphene sheet-polypyrrole based nanocomposite: synthesis, characterization and genosensing application. Dalton Transact 44:15557–15566

48. Adhikaria A, Def S, Ranab D, Natha J, Ghoshc D, Duttaa K, Chakrabortyd S, Chattopadhyayd S, Chakrabortye M, Chattopadhyaya D (2020) Selective sensing of dopamine by sodium cholate tailored polypyrrole-silver nanocomposite. Synthet Metals 260:116296

49. Riccardi CS, Kranz C, Kowalik J, Yamanaka H, Mizaikoff B, Josowicz M (2008) Label-Free DNA detection of hepatitis C virus based on modified conducting polypyrrole films at microelectrodes and atomic force microscopy tip-integrated electrodes. Anal Chem 80:237–245

50. Xu Y, Ye X, Yang L, He P, Fang Y (2006) Impedance DNA biosensor using electropolymerized polypyrrole/multiwalled carbon nanotubes modified electrode. Electroanalysis 18:1471–1478

51. Wilson J, Radhakrishnan S, Sumathi C, Dharuman V (2010) Polypyrrole-polyaniline-Au (PPy-PANi-Au) nano composite films for label-free electrochemical DNA sensing. Sens Actuators B Chem 171:216–222

52. Radhakrishnan S, Sumathi C, Umar A, Kim SJ, Wilson J, Dharuman V (2013) Polypyrrole-poly(3,4-ethylenedioxythiophene)-Ag (PPy-PEDOT-Ag) nanocomposite films for label-free electrochemical DNA sensing. Biosens Bioelectron 47:133–140